SPANDIDOS PUBLICATIONS

ONCOLOGY LETTERS 22: 657, 2021

Iron regulatory protein 1 promotes ferroptosis by sustaining cellular iron homeostasis in melanoma

FENGPING YAO[1], XIAOHONG CUI[2], YING ZHANG[1], ZHUCHUN BEI[3], HONGQUAN WANG[3], DONGXU ZHAO[1], HONG WANG[3] and YONGFEI YANG[1]

[1]School of Life Science, Beijing Institute of Technology, Beijing 100081; [2]Psychiatry Department, Shanxi Bethune Hospital, Taiyuan, Shanxi 030000; [3]State Key Laboratory of Pathogens and Biosecurity, Beijing Institute of Microbiology and Epidemiology, Beijing 100071, P.R. China

Received December 18, 2020; Accepted May 17, 2021

DOI: 10.3892/ol.2021.12918

Abstract. Melanoma, the most aggressive skin cancer, is mainly treated with BRAF inhibitors or immunotheareapy. However, most patients who initially responded to BRAF inhibitors or immunotheareapy become resistant following relapse. Ferroptosis is a form of regulated cell death characterized by its dependence on iron ions and the accumulation of lipid reactive oxygen species (ROS). Recent studies have demonstrated that ferroptosis is a good method for tumor treatment, and iron homeostasis is closely associated with ferroptosis. Iron regulatory protein (IRP)1 and 2 play important roles in maintaining iron homeostasis, but their functions in ferroptosis have not been investigated. The present study reported that the expression of IRP1 and IRP2 was increased by the ferroptosis inducers erastin and RSL3 in melanoma cells. Depletion of IRP1 significantly suppressed erastin- and RSL3-induced ferroptosis. IRP2 had a weak effect but could enhance the promoting function of IRP1 on ferroptosis. Further, erastin and RSL3 promoted the transition of aconitase 1 to IRP1, which regulated downstream iron metabolism proteins, including transferrin receptor (TFRC), ferroportin (FPN) and ferritin heavy chain 1 (FTH1). Moreover, overexpression of TFRC and knockdown of FPN and FTH1 significantly promoted erastin- and RSL3-induced ferroptosis in IRP1 knockdown melanoma cells. Collectively, the present findings indicate that IRP1 plays an essential role in erastin- and RSL3-induced ferroptosis by regulating iron homeostasis.

Correspondence to: Dr Yongfei Yang, School of Life Science, Beijing Institute of Technology, 5 South Zhong Guan Cun Street, Beijing 100081, P.R. China
E-mail: yangyf@bit.edu.cn

Dr Hong Wang, State Key Laboratory of Pathogens and Biosecurity, Beijing Institute of Microbiology and Epidemiology, 20 Dong Dajie Street, Fengtai, Beijing 100071, P.R. China
E-mail: ammswh@sina.com

Key words: iron regulatory protein 1, transferrin receptor, ferroportin, ferritin, ferroptosis, melanoma

Introduction

Iron, the most abundant trace element in the human body, is involved in various biological processes such as oxygen transport, mitochondrial respiration and DNA synthesis (1,2). Iron deficiency causes numerous types of diseases. For instance, patients with chronic kidney disease have an absolute iron deficiency, and anemia can accelerate heart disease progression and increase the risk of death (3,4). However, excess iron is also toxic and produces reactive oxygen species (ROS), leading to DNA and protein damage, lipid peroxidation and cellular death (5-7). Bilateral substantia nigra in patients with Parkinson's disease exhibit increased iron levels (8). Non-alcoholic fatty liver disease, which shows signs of elevated serum ferritin concentration, has been confirmed to be closely related to type 2 diabetes (2,9,10). Therefore, both iron deficiency and iron overload are harmful to human health, and it is essential to maintain iron homeostasis in the body.

Iron regulatory protein (IRP)1 and IRP2 are two iron regulatory proteins that play essential roles in iron metabolism. These proteins regulate the transcription of genes associated with iron metabolism by binding to iron-responsive elements (IREs) (11). IRP1 is a bifunctional enzyme that also functions as a cytosolic aconitase (ACO1) (12). When intracellular iron levels are high, ACO1 binds to the iron-sulfur (4Fe-4S) cluster and functions as an aconitase; when intracellular iron levels are low, IRP1 dissociates from the iron-sulfur cluster and functions as an iron regulatory protein (13,14). IRP1 is insensitive to cellular iron status but sensitive to oxygen, nitrogen oxides and hydroxides. With increasing oxygen concentrations, ACO1 is converted to IRP1, and its RNA-binding activity is significantly increased (15-19). In contrast, IRP2 is sensitive to iron status and can be activated on a low-iron diet (15). When IRP1 and IRP2 are activated, they bind to the 5' untranslated region (UTR) of the iron exporter protein ferroportin (FPN) and the iron storage protein ferritin to inhibit their translation, thus reducing iron export and storage (1,16). Moreover, IRP1 and IRP2 can bind to the 3'UTR of the transferrin receptor (TFRC), which is involved in iron uptake, to prevent its degradation, thereby increasing iron import (1,16).

Ferroptosis is a non-apoptotic form of cell death characterized by its dependence on iron ions and the accumulation of lipid ROS (20). Erastin and RSL3 are two small-molecule ferroptosis inducers that were originally identified by high-throughput screening (21,22). RSL3 induces ferroptosis by directly inhibiting the antioxidant enzyme glutathione peroxidase 4, which plays an essential role in removing lipid ROS (23). Erastin induces ferroptosis by inhibiting the activity of the glutamate/cystine antiporter system X_c^-, which transports cystine into cells (20). Reduced cystine intake leads to decreased glutathione synthesis, lipid ROS accumulation and ferroptosis (20). The relative intracellular levels of iron and lipid ROS are typical indicators of ferroptosis (24). Several genes that affect iron metabolism are involved in ferroptosis. For example, knockdown of FPN accelerates erastin-induced ferroptosis in neuroblastoma cells (25). Transferrin is also important for ferroptosis, and knockdown of the TFRC gene can significantly inhibit ferroptosis (26). In addition, ferritinophagy is also an effective inducer of ferroptosis. In this process, ferritin heavy chain 1 (FTH1) is degraded via autophagy, leading to increased intracellular iron and ferroptosis (27-30).

Melanoma is the most aggressive type of skin cancer, which arises from pigment-producing melanocytes (31,32). Currently, the main treatment methods for melanoma are immunotherapy and BRAF inhibitor therapy; however, numerous patients do not benefit from these methods due to immune escape and drug resistance (33). Multiple studies have shown that ferroptosis plays an essential role in melanoma cells. For example, ferroptosis inducers significantly enhance the inhibition of B16F10 tumor growth by radiotherapy or immunotherapy (34). Moreover, knockdown of the glutamate/cysteine anti-transporter significantly inhibits melanoma metastasis and improves C57BL/6-mouse survival (35).

In the present study, the human melanoma cell lines, A375 and G-361, were used to study the molecular mechanism of IRP1 and IRP2 in ferroptosis. A previous study demonstrated that oncogenic RAS mutants can increase ROS levels through the RAS-RAF-MEK-MAPK pathway (20). Both A375 and G-361 harbor the $BRAF^{V600E}$ mutation and are sensitive to ferroptosis inducers (35-38). Iron metabolism plays an important role in ferroptosis; however, the role of IRP1 in ferroptosis remains unclear. The present study used melanoma A375 and G-361 cells to investigate whether IRP1 is involved in the regulation of ferroptosis and the molecular mechanisms involved, hoping to provide a potential target for the treatment of melanoma.

Materials and methods

Cell culture. The melanoma cell lines A375 (cat. no. CRL-1619), G-361 (cat. no. CRL-1424) and human embryonic kidney cells 293T (cat. no. CRL-3216) cell lines were obtained from the American Type Culture Collection and cultured in a cell incubator with 5% CO_2 at 37˚C. Cells were cultured in DMEM containing 0.1 mg/l ferric nitrate (cat. no. 11995065, Gibco; Thermo Fisher Scientific, Inc.) with 10% FBS (Invitrogen; Thermo Fisher Scientific, Inc.) and 1% penicillin-streptomycin (Gibco; Thermo Fisher Scientific, Inc.). The universal mycoplasma detection kit (cat. no. 30-1012K; American Type Culture Collection) was used to detect mycoplasma contamination. Mycoplasma contamination was not found in any cell line.

Plasmids and transfection. To transient expression of IRP1, IRP2 and TFRC in cells, the overexpression structures of pcDNA5/FRT/TO-IRP1-Flag, pcDNA5/FRT/TO-IRP2-HA and pcDNA5/FRT/TO-TFRC-Flag were constructed. The full-length cDNA sequence of IRP1, IRP2 or TFRC was cloned into the *Afl*II and *Not*I sites of the pcDNA5/FRT/TO vector (AddGene, Inc.), and the Flag or HA sequence was cloned into the *Xho*I site of the pcDNA5/FRT/TO vector in frame with the gene coding region of IRP1, IRP2 or TFRC. To make cell lines stably expressing IRP1, IRP2 and TFRC, the pCDH/puro-IRP1-Flag, pCDH/puro-IRP2-HA and pCDH/puro-TFRC-Flag plasmids were constructed. Using pcDNA5/FRT/TO-IRP1-Flag, pcDNA5/FRT/TO-IRP2-HA and pcDNA5/FRT/TO-TFRC-Flag as templates, the tagged full length cDNA sequences were cloned and inserted into the *Xba*I and *Not*I sites of the pCDH-CMV-MCS-EF1-Puro vector (Addgene, Inc.). All constructs were confirmed by sequencing.

All shRNA targeting sequences were designed using the Broad Institute website (https://portals.broadinstitute.org/gpp/public). The miRNAs were transfected into A375 or G-361 cells using Lipofectamine® 2000 (cat. no. 11668019; Invitrogen; Thermo Fisher Scientific, Inc.) or the calcium phosphate transfection kit (cat. no. K278001, Thermo Fisher Scientific, Inc.), according to the manufacturer's instructions. Following incubation for 48 h at 37˚C, the cells were collected for subsequent analysis. The targeting sequences were as follows: i) IRP1, 5'-CCTACAAGAAAGCGGAGTCAT-3' and 5'-GCAGGATTGTTAGCAAAGAAA-3'; ii) IRP2, 5'-CCA CCCTTAGTGGTAGCTTAT-3; iii) FPN, 5'-TTGTTCAAG ACTAGCTAATTT-3'; and iv) FTH1, 5'-CCTGTCCATGTC TTACTACTT-3'. All constructs were confirmed by sequencing.

The transfection process of Lipofectamine® 2000 was as follows: Cells were seeded at a density of 70% and cultured overnight. On the second day, dilute 15 μl lipofectamine 2000 reagent with 150 μl Opti-MEM medium in a centrifuge tube and dilute 10 μg DNA constructs with 150 μl Opti-MEM medium in another tube, respectively. The diluted DNA was mixed with the diluted Lipofectamine® 2000 reagent at a ratio of 1:1 and incubated at 25˚C for 5 min. The mixture was added into the cells to be transfected. Following incubation for 48 h at 37˚C, the cells were collected for subsequent analysis.

The transfection of calcium phosphate transfection process is as follows: Cells were seeded at a density of 50% and cultured overnight. The next day, 4 h before transfection, the medium was replaced with a fresh medium containning 2% FBS. The DNA (25 μg) was mixed directly with a concentrated solution (2 M) of $CaCl_2$, which was added dropwise to a phosphate buffer to form a fine precipitate. Following incubation at 25˚C for 20 min, the precipitate was added to cells to be transfected. Following incubation for 48 h at 37˚C, cells were collected for subsequent analysis.

Antibodies and reagents. The following antibodies were used: IRP1 (cat.no.ab236773; Abcam), IRP2 (cat.no.ab232994; Abcam), TFRC (cat. no. ab214039; Abcam), FPN (cat. no. ab239583;

Abcam), ferritin heavy chain 1 (cat. no. ab183781; Abcam), HA (cat. no. H6533; Sigma-Aldrich; Merck KGaA), Flag (cat. no. F3165; clone M2; Sigma-Aldrich; Merck KGaA) and β-actin (cat. no. PA11689; Thermo Fisher Scientific, Inc.). The horseradish peroxidase (HRP)-labeled secondary antibody conjugates (cat. no. G-21040) were purchased from Thermo Fisher Scientific, Inc. Erastin (cat. no. E7781) and RSL3 (cat. no. S8155) were obtained from Selleck Chemicals.

Cell viability assay. Cell viability was evaluated using Cell Counting Kit-8 (CCK-8; cat. no. 96992; Sigma-Aldrich; Merck KGaA). This assay uses the highly water-soluble tetrazolium salt WST-8, which can be reduced by mitochondrial dehydrogenases in the presence of electron-coupled agents to produce a water-soluble formazan dye (https://www.dojindo.eu.com/TechnicalManual/Manual_CK04.pdf). Briefly, A375 or G-361 cells ($1x10^3$) were seeded in 96-well plates after being exposed to erastin (5 μM for A375 and 20 μM for G-361) or RSL3 (0.5 μM for A375 and 2 μM for G-361) at the indicated concentration at 37˚C for 24 h. The medium was then replaced with fresh medium containing 5 μl CCK-8, and the cells were returned to the incubator, and incubated for 1-4 h, according to the manufacturer's instructions, until the color of the culture medium turned orange. The absorbance was measured using a fluorescence spectrophotometer at 450 nm.

Iron assay. The intracellular content of Fe^{2+} was measured using the Iron Assay Kit (cat. no. ab83366; Abcam). The cells were collected after being treated with erastin (5 μM for A375 and 20 μM for G-361) or RSL3 (0.5 μM for A375 and 2 μM for G-361) at the indicated concentrations at 37˚C for 24 h and homogenized with iron assay buffer on ice. The samples were then centrifuged at 13,000 x g for 10 min at 4˚C, and 300 μl supernatant was collected. Iron reducer (300 μl) was added, mixed and incubated at room temperature for 30 min. A volume of 200 μl iron probes was then added and mixed thoroughly. The reaction mixture was incubated for 30 min at room temperature away from light. The absorbance was measured on a colorimetric microplate reader at 593 nm.

Malondialdehyde (MDA) assay. MDA concentrations were determined using the Lipid Peroxidation Assay Kit (cat. no. ab118970; Abcam) according to the manufacturer's instructions. The cells treated with erastin (5 μM for A375 and 20 μM for G-361) or RSL3 (0.5 μM for A375 and 2 μM for G-361) at the indicated concentrations at 37˚C for 24 h were collected, and lysis buffer was added. The cells were homogenized on ice and centrifuged at 13,000 x g for 10 min at 4˚C to obtain the supernatant. A volume of 200 μl supernatant from each sample and 600 μl thiobarbituric acid (TBA) solution was added to microcentrifuge tubes, and the samples were then incubated at 95˚C for 40 min. Samples were then cooled to room temperature on an ice bath for 10 min, and 200 μl from each reaction mixture was added to each well of a 96-well plate for analysis using a microplate reader. The absorbance of the MDA-TBA adduct was measured at 532 nm.

Detection of lipid ROS. Lipid ROS levels were analyzed by flow cytometry using the BODIPY-C11 dye (cat. no. D3861; Thermo Fisher Scientific, Inc.). The cells were treated with the indicated concentrations erastin (5 μM for A375 and 20 μM for G-361) or RSL3 (0.5 μM for A375 and 2 μM for G-361) at 37˚C for 24 h. Cells were washed with cold PBS twice and incubated in DMEM containing 5 μM BODIPY-C11 at 37˚C for 20 min. The cells were then digested with 0.25% trypsin and resuspended in PBS at with PBS to a cell density of approximately 10^6/ml. The cell suspension was filtered and immediately subjected to flow cytometry (Agilent NovoCyte Advanteon) to analyze lipid ROS levels.

ACO1 activity assay. ACO1 activity was measured using the aconitase assay kit (cat. no. ab83459; Abcam) according to the manufacturer's instructions. Briefly, 10 μl isocitrate was added to a 490 μl analytical buffer to prepare a 2 mM isocitrate standard and gradiently diluted to make a standard curve samples. The cells were collected and washed with cold PBS twice, then resuspended in assay buffer for homogenization. Cells were centrifuged at 800 x g for 10 min at 4˚C, and 100 μl supernatant was then collected into a new tube. Subsequently, 10 μl activation solution was added to the 100 μl sample, and incubated on ice for 1 h to activate ACO1. The activated samples (50 μl/well) and the standard sample (50 μl/well) were added into the 96 well plates. Add 50 μl reaction mixture (provided in the kit) to each well, and the mixture was incubated at 25˚C for 60 min. Following incubation, 10 μl developer solution was added and the mixture was incubated at 25˚C for 10 min. The absorbance was measured at a wavelength of 450 nm, using a microplate reader (Epoch™; Bio Tek).

RNA Immunoprecipitation (RIP) analysis. The IRE-binding activity of IRP1 in melanoma cells was analyzed by RIP (39). Briefly, cells expressing Flag-tagged IRP1 or HA-tagged IRP2 were lysed in 100 μl lysis buffer (25 mM Tris at pH 7.5, 300 mM NaCl, 1 mM EDTA and 1% NP40) with protease inhibitor and RNase. Then the whole-cell lysates were centrifuged at 20,000 x g for 10 min at 4˚C and incubated with 50 μl protein G magnetic beads (Bio-Rad Laboratories, Inc.) conjugated with anti-Flag antibody (cat. no. F3165; clone M2; Sigma-Aldrich; Merck KGaA) or anti-HA antibody (cat. no. H6533; Sigma-Aldrich; Merck KGaA) for 4 h at 4˚C. The immunoprecipitates were washed with RIP Wash buffer, and the RNA was extracted from the immunoprecipitation complex using 50 μg/ml Proteinase K (cat. no. P2308; Sigma-Aldrich; Merck KGaA) at 55˚C for 30 min. qPCR was performed using the iQ SYBR-Green Master Mix (Bio-Rad Laboratories, Inc.) on a CFX96 Touch Quantitative PCR Detection System (Bio-Rad Laboratories, Inc.). The following primer sequences were used for qPCR: FTH1 forward, 5'-ACTGATGAAGCTGCAGAACC-3' and reverse, 5'-GTCACCCAATTCTTTGATGG-3'; and β-actin forward, 5'-GCTCGTCGTCGACAACGGCT-3' and reverse, 5'-CAAACATGATCTGGCTCATCTTCTC-3'. The following thermocycling conditions were used for qPCR: Pre-denaturation at 94˚C for 30 sec, followed by 40 cycles of deformation at 94˚C for 5 sec, annealing at 50-60˚C for 10 sec, and extension at 72˚C for 20 sec. Relative FTH1 expression was normalized to β-actin according to the $2^{-\Delta\Delta Cq}$ method (40).

Reverse transcription-quantitative PCR analysis. Total RNA was extracted using the RNeasy Mini kit from cells

(cat. no. 74104; Qiagen GmbH). cDNA was synthesized using the iScript™ cDNA Synthesis kit (Bio-rad Laboratories, Inc.). The temperature and duration of RT were as follows: The RNA was denatured at 65˚C for 5 min, then incubated at 42˚C for 15 min and finally heated at 85˚C for 5 sec. qPCR was carried out using the iQ SYBR-Green Master Mix (Bio-rad Laboratories, Inc.) on a CFX96 Touch Quantitative PCR Detection System (Bio-Rad Laboratoreis, Inc.). The following thermocycling conditions were used for qPCR: Pre-denaturation at 94˚C for 30 sec, followed by 45 cycles of deformation at 94˚C for 5 sec, annealing at 50-60˚C for 10 sec, and extension at 72˚C for 20 sec. The quantification was determined using the $2^{-\Delta\Delta Cq}$ method (40). The gene expression levels were all normalized to β-actin. The following primer sequences were used: IRP1 forward, 5'-GTGAGT GAGAAGCAGAGTAT-3' and reverse, 5'-TGGTGGCAGTGG TAGTTA-3'; IRP2 forward, 5'-TCCATTACCAGTCATCCA TC-3' and reverse, 5'-TATCTTCCTTACCTCGTCTATC-3'; TFRC forward, 5'-GGTTATGTGGCGTATAGTAAG-3' and reverse, 5'-CTGAGTGTGATTGAAGGAAG-3'; FPN forward, 5'-ATCACAACCGCCAGAGA-3' and reverse, 5'-GCAACA ACAACAATCCAATC-3'; FTH1 forward, 5'-GCTTGGCGG AATATCTCTT-3' and reverse, 5'-AACTGAACAACGGCA CTTA-3'; and β-actin forward, 5'-GCTCGTCGTCGACAA CGGCT-3' and reverse, 5'-CAAACATGATCTGGCTCATCT TCTC-3'.

Immunoblotting. For immunoblotting, cells were washed with cold PBS twice, then lysed in lysis buffer (20 mM Tris at pH 7.5; 150 mM NaCl; 1 mM EDTA; 2% Triton X-100) supplemented with a phosphatase inhibitor mix (Pierce™; Thermo Fisher Scientific, Inc.) and a complete protease inhibitor cocktail (Roche Diagnostics). The samples were heated with SDS-PAGE loading buffer at 95˚C for 5 min. Protein concentration was determined using the Bio-Rad protein assay. The proteins were loaded equally (10 μl) onto 8% polyacrylamide gels, separated, then transferred to a PVDF membrane (Bio-Rad Laboratories, Inc.). The PVDF membrane was then blocked with 5% non-fat milk at room temperature for 30 min, then incubated with the antibodies against IRP1 (1:1,000; cat. no. ab236773; Abcam), IRP2 (1:1,000; cat. no. ab232994; Abcam), TFRC (1:1,000; cat. no. ab214039; Abcam), FPN (1:1,000; cat. no. ab239583; Abcam), FTH1 (1:1,000; cat. no. ab183781; Abcam), HA (1:1,000; cat. no. H6533; Sigma-Aldrich; Merck KgaA), Flag (1:1,000; cat. no. F3165; Sigma-Aldrich; Merck KgaA) and β-actin (1:1,000; cat. no. PA11689; Thermo Fisher Scientific, Inc.) at 4˚C for 24 h. The membranes were washed twice with PBST (PBS+1% Tween 20) and subsequently incubated with HRP-conjugated goat secondary antibodies (1:5,000; cat. no. G-21040; Thermo Fisher Scientific, Inc.) at room temperature for 1 h. The bands were visualized using the Pierce™ ECL Western Blotting Substrate (Thermo Fisher Scientific, Inc.) and densitometry analysis was performed using ImageJ software (Image-Pro Plus 6.0; National Institutes of Health).

Lentivirus production and transduction. 293T cells (the third generation) were transfected with the aforementioned plasmid constructs, pCMV-VSV-G (Addgene, Inc.) and pCMV-dR8.91 (Addgene, Inc.) at a ratio of 5:4:1 using the calcium phosphate transfection kit (cat. no. K278001, Thermo Fisher Scientific, Inc.). Viral particles were collected 48 h after transfection, filtered with a 0.45-μm sterile filter, then concentrated by ultracentrifugation at 4˚C (30,000 x g for 2 h) in a Beckman-Coulter ultracentrifuge XL-100K. The viral particles were resuspended with fresh medium, then A375 or G-361 cells were infected with viral particles (multiplicity of infection=50), the cultures were centrifuged at 25˚C (300 x g for 1 h) to facilitate the entry of viruses into cells, then incubated cells at 37˚C for 24 h. Replenished the cultures with fresh medium and maintained for another 48 h. Finally, selected the lentivirus-transduced cells with fresh medium containing 1 μg/ml puromycin for 7 days.

Statistical analysis. Data are presented as the mean ± SD. Statistical analysis was performed using GraphPad Prism 8.0 (GraphPad Software, Inc.). For multigroup comparisons, one-way ANOVA followed by Dunnett's post hoc test was used. All experiments were independently repeated three times. $P<0.05$ was considered to indicate a statistically significant difference.

Results

Expression of IRP1 and IRP2 is increased in melanoma cells treated with erastin and RSL3. To investigate whether the expression of IRP1 and IRP2 is altered in ferroptosis, the human melanoma cell lines A375 and G-361 were treated with different concentrations of erastin and RSL3 for 24 h, and the mRNA levels of IRP1 and IRP2 were analyzed using RT-qPCR. Erastin and RSL3 significantly promoted the mRNA levels of IRP1 in a dose-dependent manner (Fig. 1A and B; Fig. S1A and B). However, IRP2 expression only slightly increased compared with the DMSO-treated group. The protein levels of IRP1 and IRP2 were also by western blotting. It was observed that the protein levels of IRP1 were significantly increased following erastin and RSL3 treatment in a dose-dependent manner, whereas IRP2 protein levels only increased slightly compared with the DMSO-treated group (Fig. 1C and D; Fig. S1C and D). These findings indicate that erastin and RSL3 promote the expression of IRP1 and IRP2 in melanoma cells.

Knockdown of IRP1 significantly inhibits erastin- and RSL3-induced ferroptosis. To determine whether IRP1 and IRP2 regulate erastin- and RSL3-induced ferroptosis, IRP1, IRP2, and IRP1/2 knockdown A375 and G-361 cells using shRNA constructs. These cell lines were then treated with different concentrations of erastin and RSL3 for 24 h. It was identified that knockdown of IRP1 significantly inhibited erastin- and RSL3-induced ferroptotic cell death (Figs. 2A and S2A). Knockdown of IRP2 had a slight effect, and simultaneous knockdown of IRP1 and IRP2 demonstrated a more substantial effect on erastin- and RSL3-induced ferroptotic cell death (Figs. 2A and S2A). The intracellular concentrations of iron, MDA and lipid ROS are the main indicators of ferroptosis (24). The effect of IRP1 and IRP2 on the accumulation of Fe^{2+} was then evaluated. Knockdown of IRP1 significantly suppressed the accumulation of Fe^{2+} compared with the control group (Figs. 2B and S2B). Lipid

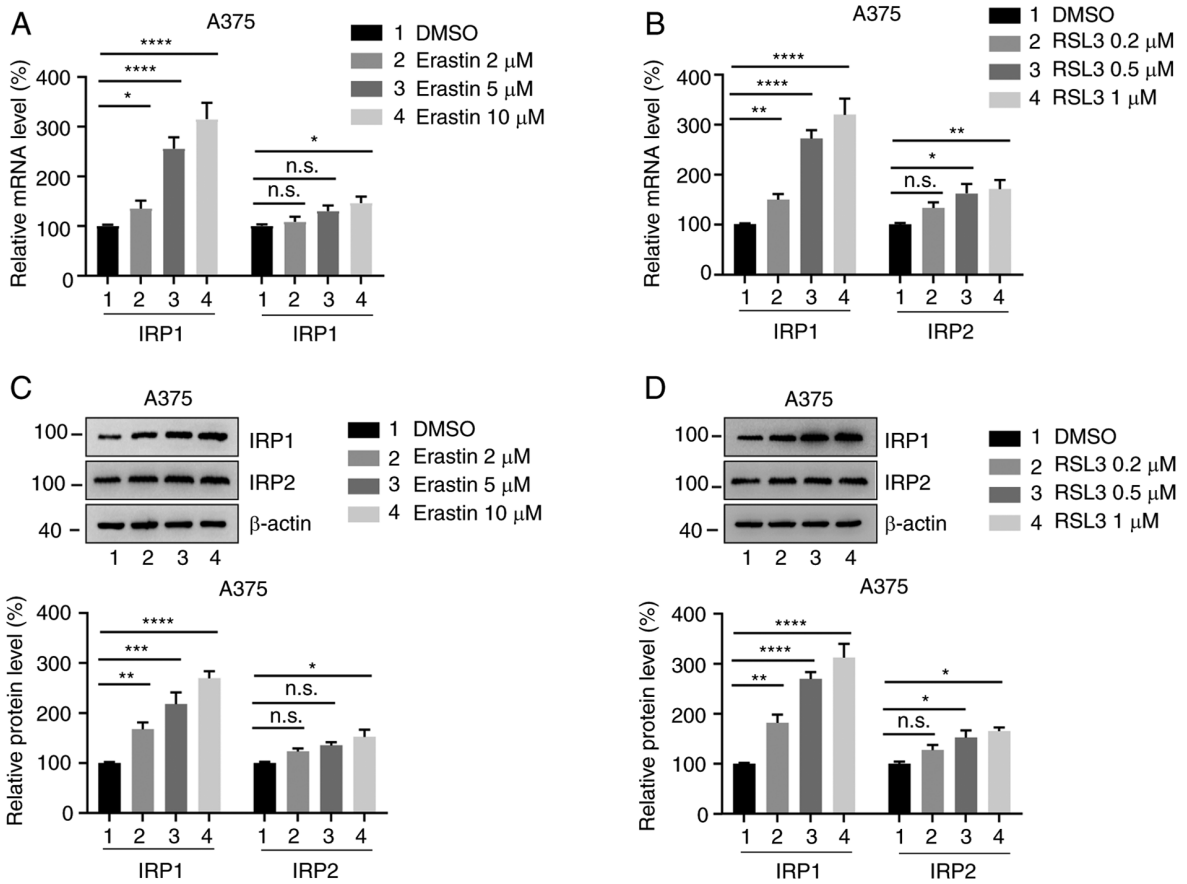

Figure 1. Erastin and RSL3 promote the expression of IRP1 and IRP2 in A375 melanoma cells. (A and B) mRNA levels of IRP1 and IRP2 were increased in (A) erastin- or (B) RSL3-treated A375 cells. (C and D) Protein levels of IRP1 and IRP2 were increased in (A) erastin- or (B) RSL3-treated A375 cells. Data are presented as the mean ± SD of three independent experiments. *P<0.05; **P<0.01; ***P<0.001; ****P<0.0001. IRP, iron regulatory protein.

peroxidation is an essential process in ferroptosis. MDA, as the end product of lipid peroxidation, is used to quantify ferroptosis (24). The levels of MDA in IRP1 knockdown cells was significantly decreased compared with the control group. Lipid ROS accumulation also reduced in IRP1 knockdown cells compared with the control group (Figs. 2D and S2D). However, the accumulation of Fe^{2+}, MDA and lipid ROS in the IRP2 knockdown cells was only slightly reduced compared with the control group (Figs. 2 and S2). The expression levels of IRP1 and IRP2 in the corresponding knockdown cell lines were significantly decreased compared with the control group (Figs. 2E and S2E).

Interestingly, simultaneous knockdown of IRP1 and IRP2 had a more substantial effect on the accumulation of Fe^{2+}, MDA and lipid ROS, suggesting that IRP1 and IRP2 have synergistic effects in ferroptosis (Figs. 2 and S2). These results indicate that knockdown of IRP1 significantly inhibits erastin- and RSL3-induced ferroptosis, which can be further promoted by IRP2 silencing.

Overexpression of IRP1 significantly promotes erastin- and RSL3-induced ferroptosis. To further confirm the role of IRP1 and IRP2 in ferroptosis, IRP1-, IRP2- and IRP1/IRP2-overexpressing A375 and G-361 cell lines were established. Cell viability was measured following treatment with different concentrations of erastin and RSL3 for 24 h. Overexpression of IRP1 significantly reduced cell viability following erastin and RSL3 treatment, while overexpression of IRP2 had a weak effect (Figs. 3A and S3A). The accumulation of iron, MDA, and lipid ROS. Consistent with the aforementioned results, the intracellular levels of Fe^{2+}, MDA and lipid ROS in IRP1-overexpressing cells were significantly increased compared with the control group (Figs. 3B-D and S3B-D). Overexpression of IRP2 had a slight effect on the accumulation of iron, MDA and lipid ROS (Figs. 3B-D and S3B-D). The expression levels of IRP1 and IRP2 in the corresponding overexpression cell lines were significantly increased compared with the control group (Figs. 3E and S3E). These findings support the essential role of IRP1 in ferroptosis induced by erastin and RSL3 and suggest that IRP2 is also involved in this process.

Erastin and RSL3 promote the conversion of ACO1 to IRP1. IRP1 is a bifunctional protein that either regulates the conversion of citrate and iso-citrate as ACO1 or regulates iron homeostasis as IRP1 (41). To verify which function mediates erastin- and RSL3-induced ferroptosis, the activity of ACO1 and the IRE binding of IRP1 were detected in transfected cells treated with erastin and RSL3. Comparing the changes in these two activities could reveal the transition between ACO1 and IRP1 in response to erastin and RSL3.

As shown in Fig. 4A and B, as well as S4A and B, there was a significant decrease in ACO1 activity and a substantial increase of IRE-binding activity upon erastin

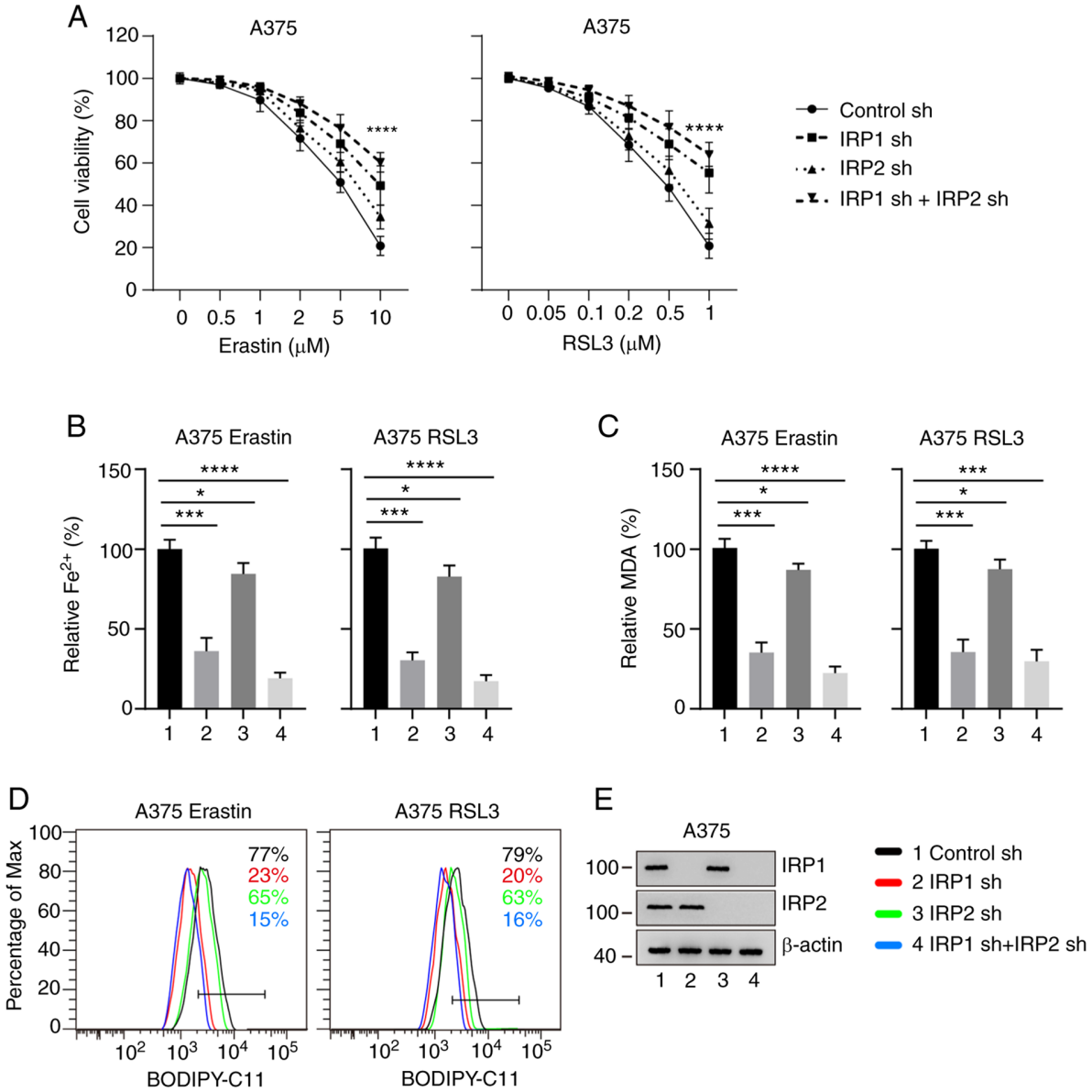

Figure 2. Knockdown of IRP1 and IRP2 inhibits erastin- and RSL3-induced ferroptosis. (A) IRP1 and IRP2 knockdown inhibited erastin- and RSL3-induced ferroptotic cell death in A375 melanoma cells. (B) Knockdown of IRP1 and IRP2 inhibited erastin- and RSL3-induced iron accumulation in A375 cells. (C and D) Knockdown of IRP1 and IRP2 suppressed erastin- and RSL3-induced (C) MDA and (D) lipid ROS accumulation. The black line represents the control cells; the red line represents IRP1 knockdown; the green line represents IRP2knockdown and the blue line represents IRP1 and IRP2 knockdown. (E) Protein levels of IRP1 and IRP2 were detected following IRP1 and IRP2 knockdown. Data are presented as the mean ± SD of three independent experiments. *P<0.05; ***P<0.001; ****P<0.0001. IRP, iron regulatory protein. IRP, iron regulatory protein; sh, short hairpin RNA.

and RSL3 treatment in the control cells, and IRP2 cells, rather than IRP1 knockdown cells, or IRP1/IRP2 simultaneously knockdown cells, suggesting that erastin and RSL3 facilitated the transition of ACO1 to IRP1 and the transition depends on IRP1. Knockdown of IRP1 strongly suppressed the activity of ACO1 and IRP1, and the transition of ACO1 to IRP1 induced by erastin or RSL3 was also significantly inhibited (Fig. 4A and B; Fig. S4A and B). Consistent with the aforementioned results, the transition of ACO1 to IRP1 was also eliminated in IRP1 and IRP2 knockdown cells, as evidenced by the lack of change in the activity of ACO1 and IRE binding (Fig. 4A and B; Fig. S4A and B). However, the changes in ACO1 activity and IRE binding in IRP2 knockdown cells were similar to the control cells, suggesting that IRP2 has no significant impact on the transition of ACO1 to IRP1 under basal conditions or in response to erastin and RSL3 (Fig. 4A and B; Fig. S4A and B). Unlike IRP1, the IRE binding of IRP2 was not affected by erastin or RSL3 (Figs. 4C and S4C). These data suggest that erastin and RSL3 can significantly facilitate the transition of ACO1 to IRP1 and that the IRE binding activity of IRP1 is significantly increased during ferroptosis.

IRP1 regulates the expression of iron metabolism proteins during ferroptosis. IRP1 regulates iron homeostasis by post-transcriptionally modifying proteins involved in iron metabolism, such as TFRC, FPN and ferritin (1,42-44). To further explore the molecular mechanism underlying IRP1 in erastin- and RSL3-induced ferroptosis, the expression levels of TFRC, FPN and FTH1 were analyzed in

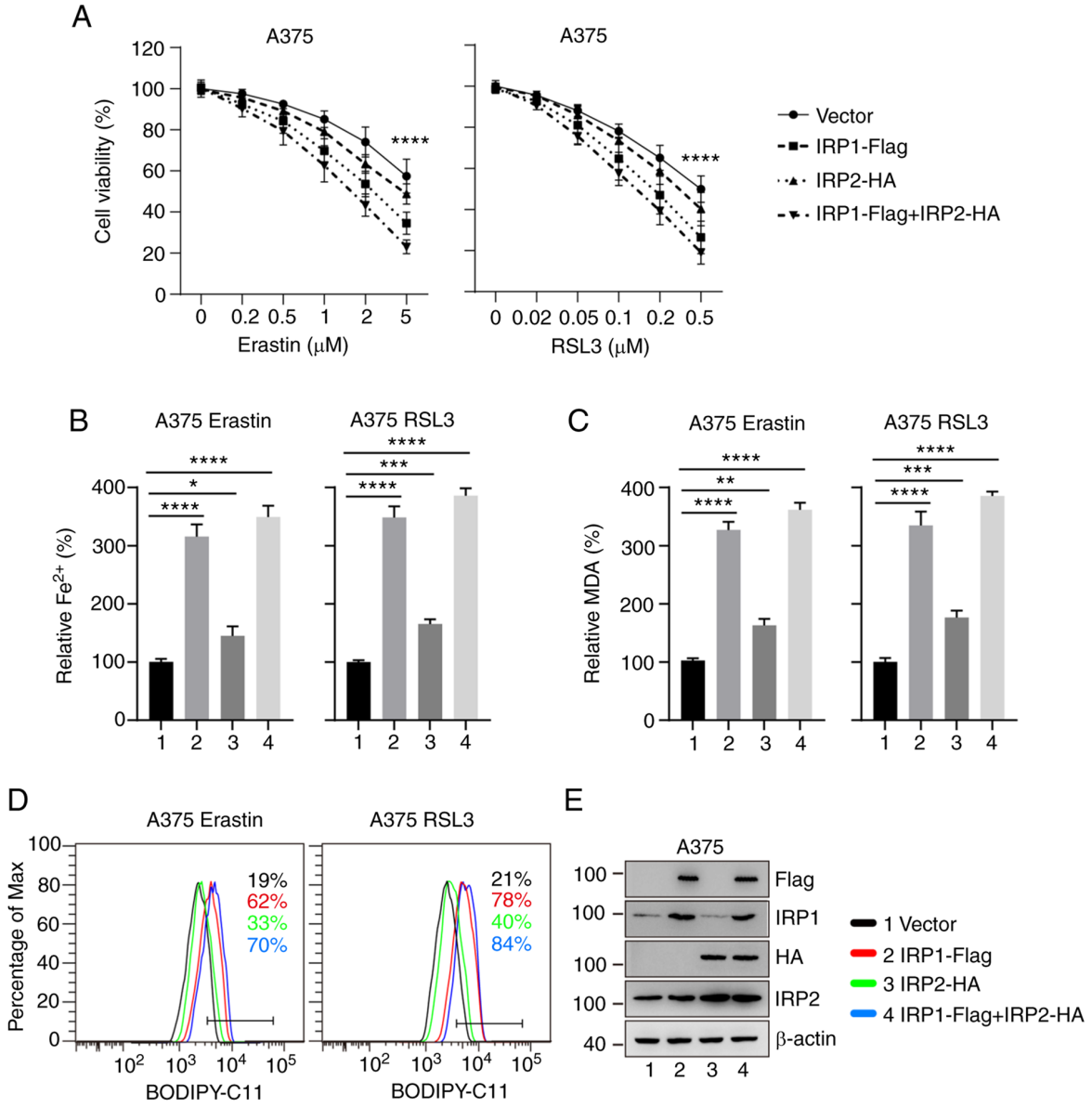

Figure 3. Overexpression of IRP1 and IRP2 promotes erastin- and RSL3-induced ferroptosis. (A) IRP1 and IRP2 overexpression promoted erastin- and RSL3-induced ferroptotic cell death in A375 melanoma cells. (B) Overexpression of IRP1 and IRP2 increased erastin- and RSL3-induced iron accumulation in A375 cells. (C and D) Overexpression of IRP1 and IRP2 promoted erastin- and RSL3-induced (C) MDA and (D) lipid ROS accumulation. The black line represents the control cells; the red line represents overexpression of IRP1; the green line represents overexpression of IRP2 andthe blue line represents overexpression of IRP1 and IRP2. (E) Protein levels of IRP1 and IRP2 were detected following IRP1 and IRP2 overexpression. Data are presented as the mean ± SD of three independent experiments. *P<0.05; **P<0.01; ***P<0.001; ****P<0.0001. IRP, iron regulatory protein; MDA, malondialdehyde; HA, hemagglutinin.

control sh cells and IRP1 knockdown cells. As shown in Figs. 5A and S5A, erastin and RSL3 increased the mRNA levels of TFRC in control sh cells cells. Knockdown of IRP1 had no significant effect on the mRNA expression of TFRC in DMSO-treated cells, but significantly inhibited TFRC mRNA level in erastin and RSL3 treated cells compared with DMSO-treated cells (Figs. 5A and S5A). The protein levels of TFRC was upregulated in erastin and RSL3 treated control sh cells compared with DMS-treated cells, but not in IRP1-deficient cells (Figs. 5D and S5D). Therefore, the upregulation of TFRC in erastin- and RSL3-induced ferroptosis requires IRP1. The expression levels of FPN and FTH1, which are silenced by IRPs at the post-translational level (11), were then detected. Although the mRNA levels of FPN and FTH1 had no significant increase upon erastin or RSL3 treatment compared with the DMSO treated group, (Fig. 5B, C, S5B, and SC), erastin and RSL3 decreased the protein levels of FPN and FTH1 in control sh cells but not in IRP1 knockdown cells (Figs. 5D and S5D). Therefore, IRP1 can regulate the protein expression of TFRC, FPN and FTH1 during ferroptosis.

The function of IRP1 in ferroptosis is dependent on iron metabolism proteins. Given that IRP1 regulates the protein expression of TFRC, FPN and FTH1 (11), it was hypothesized that the function of IRP1 in erastin- and RSL3-induced ferroptosis may be dependent on these iron metabolism proteins. To test this hypothesis, TFRC was overexpressed in IRP1 knockdown cells. The overexpression of TFRC strongly reduced cell viability in IRP1 knockdown cells,

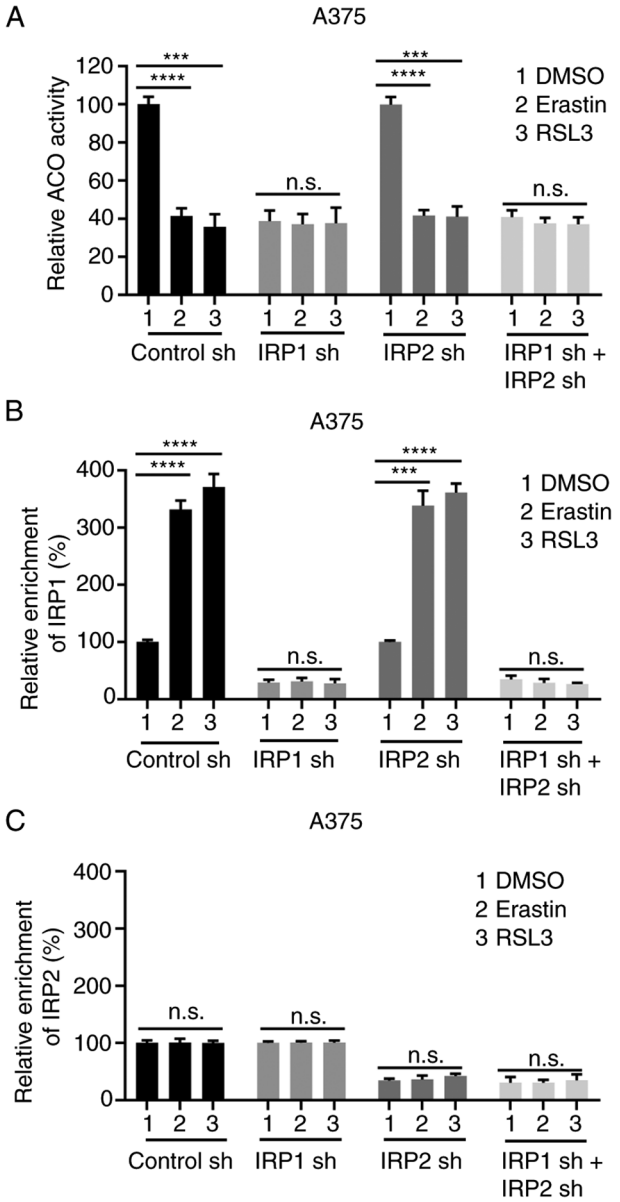

Figure 4. Erastin and RSL3 promote the transition of ACO to IRP1. (A) ACO activity decreased significantly in A375 melanoma cells following erastin and RSL3 treatment. (B) Erastin and RSL3 promoted the IRE-binding activity of IRP1. (C) Erastin and RSL3 had no significant effect on the IRE-binding activity of IRP2. The relative abundances of IRP1-Flag and IRP2-Flag were analyzed by RNA immunoprecipitation. Data are presented as the mean ± SD of three independent experiments. ***P<0.001; ****P<0.0001. ACO, aconitase; IRP, iron regulatory protein; IRE, iron-responsive element; sh, short hairpin RNA; n.s., not significant.

compared with IRP1 alone (Figs. 6A and S6A). It was also hypothesized that overexpression of TFRC could affect iron accumulation and lipid ROS production in IRP1 knockdown cells. As shown in Figs. 6B-D and S6B-D, overexpression of TFRC significantly enhanced iron accumulation, MDA and lipid ROS production in IRP1 knockdown cells, compared with IRP1 alone. TFRC expression significantly increased in TFRC overexpression cell lines (Figs. 6E, S6E and SF). Similarly, knockdown of FPN and FTH1 significantly reduced cell viability in IRP1 knockdown cells, compared with IRP1 alone (Figs. 6 and S6). As expected, the simultaneous overexpression of TFRC and knockdown of FPN and FTH1 could almost eliminate the inhibitory effect of IRP1 knockdown on erastin- and RSL3-induced ferroptosis in melanoma cells (Figs. 6 and S6). Therefore, these results indicate that IRP1 plays a crucial role in ferroptosis by regulating iron metabolism proteins.

Discussion

In the present study, IRP1 promoted ferroptosis by regulating iron homeostasis. The expression of IRP1 significantly increased in melanoma cells following treatment with erastin and RSL3. Increased IRP1 levels could promote the expression of TFRC and inhibit the translation of FPN and FTH1, which further increased the intracellular iron levels to promote ferroptosis. In the absence of IRP1, the accumulation of intracellular iron was suppressed, and cells were insensitive to ferroptosis inducers (Fig. 7).

The role of IRP1 and IRP2 in iron homeostasis is well-documented. IRP2 was previously speculated to be a major regulator of iron homeostasis, since IRP1 is insensitive to changes in iron levels, and knockdown of IRP1 does not lead to overall dysregulation of iron metabolism to the same extent as knockdown of IRP2 (15,45). However, under the condition of oxidative stress, ACO1 disassociates from Fe-S clusters and is converted into IRP1, significantly increasing IRP1, and IRP1 plays a key role in iron regulation (16-18). For example, with increasing oxygen concentration, IRP1 is activated and can be a major source of IRE-binding activity (16). IRP1 is also superior to IRP2 in regulating cellular iron homeostasis in response to nitric oxide (18). Nitric oxide stimulates the disassembly of the Fe-S cluster in IRP1, leading to the activation of IRP1 (18). In IRP2 knockout mice, nitroxide tempol prevents the symptoms of neurodegenerative disease by activating IRP1 activity (17). In the present study, IRP1 expression increased more significantly in erastin- and RSL3-treated cells than IRP2. Although IRP2 is also involved in the regulation of iron homeostasis, IRP1 plays a major role in this process. Knockdown of IRP1 showed a more robust phenotype, including ferroptotic cell death, iron accumulation and lipid ROS accumulation, further confirming that IRP1 plays a major role in iron metabolism under stress conditions.

IRP1 is a bifunctional protein, which can plays a role in iron homeostasis regulation as an iron regulatory protein or participates in mitochondrial metabolism as ACO1. The present study demonstrated that the aconitase activity of ACO1 was reduced and the IRE-binding activity of IRP1 was increased in erastin- and RSL3-induced ferroptosis. These results suggested that erastin and RSL3 may facilitate the transition of ACO1 to IRP1. ACO1, a metabolic enzyme in the TCA cycle, is also sensitive to ROS (13,46,47). Under oxidative stress, ACO1 activity is reduced (48). It is possible that the accumulated lipid ROS suppresses the ACO1 activity of ACO1. To detect whether the reduction of enzyme activity is also related to the conversion of ACO1 to IRP1, the activity of IRP1 was analyzed using RIP. IRP1 was more enriched on the IRE sequences compared with the DMSO treated group, and the expression levels of TFRC, FPN and Ft were also changed. Therefore, lipid ROS may directly inhibit the activity of ACO1 or indirectly suppress the activity of ACO1 by promoting the conversion of ACO1 to IRP1.

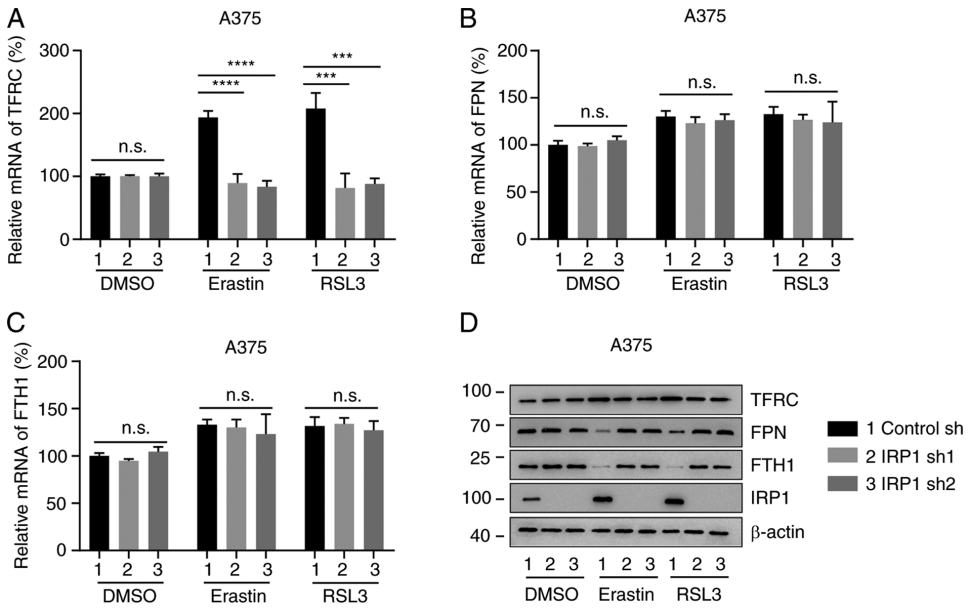

Figure 5. IRP1 is essential for the expression of iron-regulating proteins in ferroptosis. (A) Knockdown of IRP1 suppressed the mRNA expression levels expression of TFRC in A375 melanoma cells following erastin and RSL3 treatment. (B and C) Knockdown of IRP1 had no significant effect on the mRNA expression levels of (B) FPN and (C) FTH1 following erastin and RSL3 treatment. (D) Protein levels of TFRC, FPN and FTH1 in A375 cells treated with erastin or RSL3. Data are presented as the mean ± SD of three independent experiments. ***P<0.001; ****P<0.0001. IRP, iron regulatory protein; TFRC, transferrin receptor; FPN, ferroportin; FTH1, ferritin heavy chain 1; sh, short hairpin RNA; n.s., not significant.

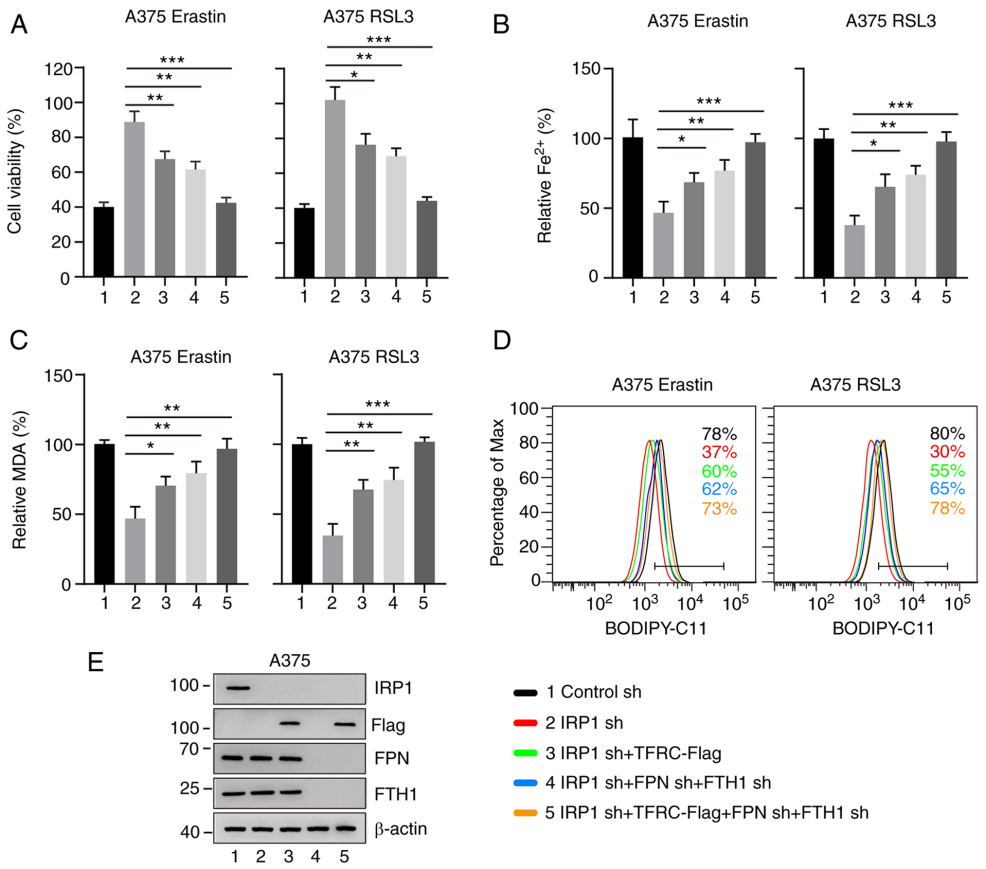

Figure 6. IRP1 function in ferroptosis depends on TFRC, FPN and FTH1. (A) Overexpression of TFRC and knockdown of FPN and FTH1 enhanced erastin- and RSL3-induced ferroptotic cell death in IRP1 knockdown A375 melanoma cells. (B) Overexpression of TFRC and knockdown of FPN and FTH1 promoted erastin- and RSL3-induced iron accumulation in IRP1 knockdown A375 melanoma cells. (C and D) Overexpression of TFRC and knockdown of FPN and FTH1 promoted erastin- and RSL3-induced (C) MDA accumulation and (D) lipid ROS accumulation in IRP1 knockdown A375 melanoma cells. The black line represents the control cells; the red line represents IRP1 knockdown; the green line represents overexpression of TFRC and IRP1 knockdown; the blue line represents the FPN, FTH1 and IRP1 knockdown and the orange line represents overexpression of TFRC and FPN, FTH1 and IRP1 knockdown. (E) Protein levels of IRP1, TFRC, FPN and FTH1 in A375 cells transfected with the indicated constructs. Data are presented as the mean ± SD of three independent experiments. *P<0.05; **P<0.01; ***P<0.001. IRP, iron regulatory protein; TFRC, transferrin receptor; FPN, ferroportin; FTH1, ferritin heavy chain 1; sh, short hairpin RNA; MDA, malondialdehyde; n.s., not significant.

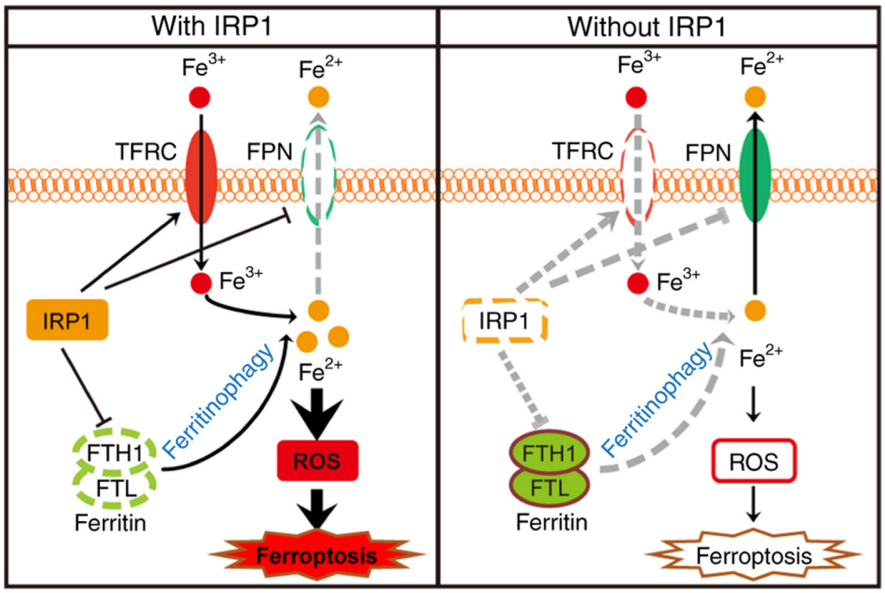

Figure 7. Schematic depicting IRP1-mediated ferroptosis in melanoma cells. The Fe^{3+} transported into cells by TFRC and the Fe^{2+} released through ferritinophagy are the main sources of iron pools. In wild-type cells, erastin- and RSL3-induced IRP1 promotes the expression of TFRC and suppresses the expression of FPN and ferritin, which increases the intracellular Fe^{2+} levels and promotes ferroptosis. In the absence of IRP1, these effects are reversed, resulting in significantly decreased intracellular Fe^{2+} levels, thus suppressing erastin- and RSL3-induced ferroptosis. IRP, iron regulatory protein; TFRC, transferrin receptor; FPN, ferroportin; FTH1, ferritin heavy chain 1; ROS, reactive oxidant species; FTL, ferritin light chain.

Furthermore, the present study demonstrated that overexpression of IRP1 increases the susceptibility of melanoma cells to ferroptosis. Previous studies have reported that mutant p53 regulates ferroptosis independently of IRPs (49-51). This contradictory result may be due to the difference between the wild-type and mutant p53 genes, and previous studies have reported the same results (52-55). For example, knockdown of spermine N1-acetyltransferase 1 in p53 wild-type tumors significantly enhanced the resistance of cells to ferroptosis, but not in p53 mutant tumors (52). Wild-type p53 can markedly enhance the sensitivity of tumor cells to ferroptosis by inhibiting solute carrier family 7 member 11 (SLC7A11), while the sensitivity of tumor cells to ferroptosis is decreased and the repression of p53 on SLC7A11 is impaired in p534KR98-expressing cells (53-55). Since tumor cells expressing wild-type or mutated p53 may have different sensitivities to ferroptosis, p53 mutational status may be an important factor to consider in the treatment of tumors with ferroptosis. Although therapies that target ferroptosis are not yet available for the treatment of tumors due to the low targeting and short half-life of ferroptosis inducers, ferroptosis is a promising treatment for tumors. Nanotechnology may also provide a technical platform for the use of ferroptosis in melanoma treatment (56-58).

In conclusion, overexpression of IRP1 increases the susceptibility of melanoma cells to ferroptosis, suggesting that patients with high expression of IRP1 may benefit more from ferroptosis treatment. Since iron homeostasis is very similar in different cancer cell types (59-62), the function and IRP1 in ferroptosis identified in melanoma may be extended to other tumors as well. Considering that several tumor types, especially drug-resistant tumors, are sensitive to ferroptosis inducers, the activation of IRP1 may represent a new therapeutic method for the treatment of tumors.

Acknowledgements

Not applicable.

Funding

The present study was supported by The National Natural Science Foundation of China (grant nos. 81772915 and 82073022).

Availability of data and materials

The datasets used and analyzed during the present study are available from the corresponding author upon reasonable request.

Authors' contributions

FY performed the experiments and analyzed the data. XC, YZ participated in the data processing, ZB participated in data interpretation and HW participated in the manuscript drafting. DZ, HQW and HW performed the experiments and analyzed the data. YY designed the experiments, analyzed the data and drafted the initial manuscript. XC, YZ confirmed the authenticity of all the raw data. All authors have read and approved the final manuscript.

Ethics approval and consent to participate

Not applicable.

Patient consent for publication

Not applicable.

Competing interests

The authors declare that they have no competing interests.

References

1. Hentze MW, Muckenthaler MU, Galy B and Camaschella C: Two to tango: Regulation of Mammalian iron metabolism. Cell 142: 24-38, 2010.
2. Datz C, Müller E and Aigner E: Iron overload and non-alcoholic fatty liver disease. Minerva Endocrinol 42: 173-183, 2017.
3. Babitt JL and Lin HY: Mechanisms of anemia in CKD. J Am Soc Nephrol 23: 1631-1634, 2012.
4. Keith DS, Nichols GA, Gullion CM, Brown JB and Smith DH: Longitudinal follow-up and outcomes among a population with chronic kidney disease in a large managed care organization. Arch Intern Med 164: 659-663, 2004.
5. Bush AI: The metallobiology of Alzheimer's disease. Trends Neurosci 26: 207-214, 2003.
6. Singh A, Kukreti R, Saso L and Kukreti S: Oxidative Stress: A Key Modulator in Neurodegenerative Diseases. Molecules 24: 1583, 2019.
7. Zager RA: Parenteral iron compounds: Potent oxidants but mainstays of anemia management in chronic renal disease. Clin J Am Soc Nephrol (Suppl 1): S24-S31, 2006.
8. Jin L, Wang J and Zhao L: Decreased serum ceruloplasmin levels characteristically aggravate nigral iron deposition in Parkinson's disease. Brain 134: 50-58, 2011.
9. Britton LJ, Subramaniam VN and Crawford DH: Iron and non-alcoholic fatty liver disease. World J Gastroenterol 22: 8112-8122, 2016.
10. Jiang R, Manson JE, Meigs JB, Ma J, Rifai N and Hu FB: Body iron stores in relation to risk of type 2 diabetes in apparently healthy women. JAMA 291: 711-717, 2004.
11. Wilkinson N and Pantopoulos K: The IRP/IRE system in vivo: Insights from mouse models. Front Pharmacol 5: 176, 2014.
12. Brown NM, Kennedy MC, Antholine WE, Eisenstein RS and Walden WE: Detection of a [3Fe-4S] cluster intermediate of cytosolic aconitase in yeast expressing iron regulatory protein 1. Insights into the mechanism of Fe-S cluster cycling. J Biol Chem 277: 7246-7254, 2002.
13. Lushchak OV, Piroddi M, Galli F and Lushchak VI: Aconitase post-translational modification as a key in linkage between Krebs cycle, iron homeostasis, redox signaling, and metabolism of reactive oxygen species. Redox Rep 19: 8-15, 2014.
14. Tong WH and Rouault TA: Metabolic regulation of citrate and iron by aconitases: Role of iron-sulfur cluster biogenesis. Biometals 20: 549-564, 2007.
15. Meyron-Holtz EG, Ghosh MC, Iwai K, LaVaute T, Brazzolotto X, Berger UV, Land W, Ollivierre-Wilson H, Grinberg A, Love P and Rouault TA: Genetic ablations of iron regulatory proteins 1 and 2 reveal why iron regulatory protein 2 dominates iron homeostasis. EMBO J 23: 386-395, 2004.
16. Meyron-Holtz EG, Ghosh MC and Rouault TA: Mammalian tissue oxygen levels modulate iron-regulatory protein activities in vivo. Science 306: 2087-2090, 2004.
17. Ghosh MC, Tong WH, Zhang D, Ollivierre-Wilson H, Singh A, Krishna MC, Mitchell JB and Rouault TA: Tempol-mediated activation of latent iron regulatory protein activity prevents symptoms of neurodegenerative disease in IRP2 knockout mice. Proc Natl Acad Sci USA 105: 12028-12033, 2008.
18. Stys A, Galy B, Starzynski RR, Smuda E, Drapier JC, Lipiński P and Bouton C: Iron regulatory protein 1 outcompetes iron regulatory protein 2 in regulating cellular iron homeostasis in response to nitric oxide. J Biol Chem 286: 22846-22854, 2011.
19. Dev S, Kumari S, Singh N, Kumar Bal S, Seth P and Mukhopadhyay CK: Role of extracellular Hydrogen peroxide in regulation of iron homeostasis genes in neuronal cells: Implication in iron accumulation. Free Radic Biol Med 86: 78-89, 2015.
20. Dixon SJ, Lemberg KM, Lamprecht MR, Skouta R, Zaitsev EM, Gleason CE, Patel DN, Bauer AJ, Cantley AM, Yang WS, *et al*: Ferroptosis: An iron-dependent form of nonapoptotic cell death. Cell 149: 1060-1072, 2012.
21. Dolma S, Lessnick SL, Hahn WC and Stockwell BR: Identification of genotype-selective antitumor agents using synthetic lethal chemical screening in engineered human tumor cells. Cancer Cell 3: 285-296, 2003.
22. Yang WS and Stockwell BR: Synthetic lethal screening identifies compounds activating iron-dependent, nonapoptotic cell death in oncogenic-RAS-harboring cancer cells. Chem Biol 15: 234-245, 2008.
23. Yang WS, SriRamaratnam R, Welsch ME, Shimada K, Skouta R, Viswanathan VS, Cheah JH, Clemons PA, Shamji AF, Clish CB, *et al*: Regulation of ferroptotic cancer cell death by GPX4. Cell 156: 317-331, 2014.
24. Wang H, An P, Xie E, Wu Q, Fang X, Gao H, Zhang Z, Li Y, Wang X, Zhang J, *et al*: Characterization of ferroptosis in murine models of hemochromatosis. Hepatology 66: 449-465, 2017.
25. Geng N, Shi BJ, Li SL, Zhong ZY, Li YC, Xua WL, Zhou H and Cai JH: Knockdown of ferroportin accelerates erastin-induced ferroptosis in neuroblastoma cells. Eur Rev Med Pharmacol Sci 22: 3826-3836, 2018.
26. Gao M, Monian P, Quadri N, Ramasamy R and Jiang X: Glutaminolysis and transferrin regulate ferroptosis. Mol Cell 59: 298-308, 2015.
27. Mancias JD, Wang X, Gygi SP, Harper JW and Kimmelman AC: Quantitative proteomics identifies NCOA4 as the cargo receptor mediating ferritinophagy. Nature 509: 105-109, 2014.
28. Zhang Z, Yao Z, Wang L, Ding H, Shao J, Chen A, Zhang F and Zheng S: Activation of ferritinophagy is required for the RNA-binding protein ELAVL1/HuR to regulate ferroptosis in hepatic stellate cells. Autophagy 14: 2083-2103, 2018.
29. Lin LS, Song J, Song L, Ke K, Liu Y, Zhou Z, Shen Z, Li J, Yang Z, Tang W, *et al*: Simultaneous Fenton-like ion delivery and glutathione depletion by MnO_2-based nanoagent to enhance chemodynamic therapy. Angew Chem Int Ed Engl 57: 4902-4906, 2018.
30. Sui S, Zhang J, Xu S, Wang Q, Wang P and Pang D: Ferritinophagy is required for the induction of ferroptosis by the bromodomain protein BRD4 inhibitor (+)-JQ1 in cancer cells. Cell Death Dis 10: 331, 2019.
31. Siegel RL, Miller KD and Jemal A: Cancer statistics, 2020. CA: Cancer J Clin 70: 7-30, 2020.
32. Brenner M and Hearing VJ: The protective role of melanin against UV damage in human skin. Photochem Photobiol 84: 539-549, 2008.
33. Armstrong JL, Corazzari M, Martin S, Pagliarini V, Falasca L, Hill DS, Ellis N, Al Sabah S, Redfern CP, Fimia GM, *et al*: Oncogenic B-RAF signaling in melanoma impairs the therapeutic advantage of autophagy inhibition. Clin Cancer Res 17: 2216-2226, 2011.
34. Lang X, Green MD, Wang W, Yu J, Choi JE, Jiang L, Liao P, Zhou J, Zhang Q, Dow A, *et al*: Radiotherapy and immunotherapy promote tumoral lipid oxidation and ferroptosis via synergistic repression of SLC7A11. Cancer Discov 9: 1673-1685, 2019.
35. Sato M, Onuma K, Domon M, Hasegawa S, Suzuki A, Kusumi R, Hino R, Kakihara N, Kanda Y, Osaki M, *et al*: Loss of the cystine/glutamate antiporter in melanoma abrogates tumor metastasis and markedly increases survival rates of mice. Int J Cancer 147: 3224-3235, 2020.
36. Konieczkowski DJ, Johannessen CM, Abudayyeh O, Kim JW, Cooper ZA, Piris A, Frederick DT, Barzily-Rokni M, Straussman R, Haq R, *et al*: A melanoma cell state distinction influences sensitivity to MAPK pathway inhibitors. Cancer Discov 4: 816-827, 2014.
37. Luo M, Wu L, Zhang K, Wang H, Zhang T, Gutierrez L, O'Connell D, Zhang P, Li Y, Gao T, *et al*: miR-137 regulates ferroptosis by targeting glutamine transporter SLC1A5 in melanoma. Cell Death Differ 25: 1457-1472, 2018.
38. Tsoi J, Robert L, Paraiso K, Galvan C, Sheu KM, Lay J, Wong DJL, Atefi M, Shirazi R, Wang X, *et al*: Multi-stage differentiation defines melanoma subtypes with differential vulnerability to drug-induced iron-dependent oxidative stress. Cancer Cell 33: 890-904.e5, 2018.
39. Miyazawa M, Bogdan AR and Tsuji Y: Perturbation of iron metabolism by cisplatin through inhibition of iron regulatory protein 2. Cell Chem Biol 26: 85-97.e4, 2019.
40. Livak KJ and Schmittgen TD: Analysis of relative gene expression data using real-time quantitative PCR and the 2(-Delta Delta C(T)) method. Methods 25: 402-408, 2001.
41. Philpott CC, Klausner RD and Rouault TA: The bifunctional iron-responsive element binding protein/cytosolic aconitase: The role of active-site residues in ligand binding and regulation. Proc Natl Acad Sci USA 91: 7321-7325, 1994.
42. Eisenstein RS: Iron regulatory proteins and the molecular control of mammalian iron metabolism. Annu Rev Nutr 20: 627-662, 2000.

43. Wallander ML, Leibold EA and Eisenstein RS: Molecular control of vertebrate iron homeostasis by iron regulatory proteins. Biochim Biophys Acta 1763: 668-689, 2006.
44. Hentze MW, Muckenthaler MU and Andrews NC: Balancing acts: Molecular control of mammalian iron metabolism. Cell 117: 285-297, 2004.
45. LaVaute T, Smith S, Cooperman S, Iwai K, Land W, Meyron-Holtz E, Drake SK, Miller G, Abu-Asab M, Tsokos M, *et al*: Targeted deletion of the gene encoding iron regulatory protein-2 causes misregulation of iron metabolism and neurodegenerative disease in mice. Nat Genet 27: 209-214, 2001.
46. Velsor LW, Kariya C, Kachadourian R and Day BJ: Mitochondrial oxidative stress in the lungs of cystic fibrosis transmembrane conductance regulator protein mutant mice. Am J Respir Cell Mol Biol 35: 579-586, 2006.
47. Gardner PR: Aconitase: Sensitive target and measure of superoxide. Methods Enzymol 349: 9-23, 2002.
48. Gardner PR, Nguyen DD and White CW: Aconitase is a sensitive and critical target of oxygen poisoning in cultured mammalian cells and in rat lungs. Proc Natl Acad Sci USA 91: 12248-12252, 1994.
49. Funauchi Y, Tanikawa C, Yi Lo PH, Mori J, Daigo Y, Takano A, Miyagi Y, Okawa A, Nakamura Y and Matsuda K: Regulation of iron homeostasis by the p53-ISCU pathway. Sci Rep 5: 16497, 2015.
50. Zhang F, Wang W, Tsuji Y, Torti SV and Torti FM: Post-transcriptional modulation of iron homeostasis during p53-dependent growth arrest. J Biol Chem 283: 33911-33918, 2008.
51. Thompson LR, Oliveira TG, Hermann ER, Chowanadisai W, Clarke SL and Montgomery MR: Distinct TP53 mutation types exhibit increased sensitivity to ferroptosis independently of changes in iron regulatory protein activity. Int J Mol Sci 21: 6751, 2020.
52. Ou Y, Wang SJ, Li D, Chu B and Gu W: Activation of SAT1 engages polyamine metabolism with p53-mediated ferroptotic responses. Proc Natl Acad Sci USA 113: E6806-E6812, 2016.
53. Jiang L, Kon N, Li T, Wang SJ, Su T, Hibshoosh H, Baer R and Gu W: Ferroptosis as a p53-mediated activity during tumour suppression. Nature 520: 57-62, 2015.
54. Jennis M, Kung CP, Basu S, Budina-Kolomets A, Leu JI, Khaku S, Scott JP, Cai KQ, Campbell MR, Porter DK, *et al*: An African-specific polymorphism in the TP53 gene impairs p53 tumor suppressor function in a mouse model. Genes Dev 30: 918-930, 2016.
55. Wang SJ, Li D, Ou Y, Jiang L, Chen Y, Zhao Y and Gu W: Acetylation is crucial for p53-mediated ferroptosis and tumor suppression. Cell Rep 17: 366-373, 2016.
56. Li J, Li J, Pu Y, Li S, Gao W and He B: PDT-Enhanced ferroptosis by a polymer nanoparticle with pH-activated singlet oxygen generation and superb biocompatibility for cancer therapy. Biomacromolecules 22: 1167-1176, 2021.
57. Jasim KA and Gesquiere AJ: Ultrastable and biofunctionalizable conjugated polymer nanoparticles with encapsulated iron for ferroptosis assisted chemodynamic therapy. Mol Pharm 16: 4852-4866, 2019.
58. Kim SE, Zhang L, Ma K, Riegman M, Chen F, Ingold I, Conrad M, Turker MZ, Gao M, Jiang X, *et al*: Ultrasmall nanoparticles induce ferroptosis in nutrient-deprived cancer cells and suppress tumour growth. Nat Nanotechnol 11: 977-985, 2016.
59. Wang Y, Yu L, Ding J and Chen Y: Iron metabolism in cancer. Int J Mol Sci 20: 95, 2018.
60. Bian Z, Hann HW, Ye Z, Yin C, Wang Y, Fang W, Wan S, Wang C and Tao K: Ferritin level prospectively predicts hepatocarcinogenesis in patients with chronic hepatitis B virus infection. Oncol Lett 16: 3499-3508, 2018.
61. Song A, Eo W, Kim S, Shim B and Lee S: Significance of serum ferritin as a prognostic factor in advanced hepatobiliary cancer patients treated with Korean medicine: A retrospective cohort study. BMC Complement Altern Med 18: 176, 2018.
62. Guo W, Zhang S, Chen Y, Zhang D, Yuan L, Cong H and Liu S: An important role of the hepcidin-ferroportin signaling in affecting tumor growth and metastasis. Acta Biochim Biophys Sin (Shanghai) 47: 703-715, 2015.